JOURNAL OF
THE ENGINEERING
MECHANICS DIVISION

MICROMECHANICS MODEL FOR CREEP OF ANISOTROPIC CLAY

By Zdeněk P. Bažant,[1] M. ASCE, I. Kutay Ozaydin,[2] and Raymond J. Krizek,[3] M. ASCE

INTRODUCTION

A more fundamental understanding of the macroscopic stress-strain behavior of clay can be achieved by studying the micromechanics of deformation. Although various hypotheses have been advanced over the years to characterize the microstructure of clay, it is only recently that a creep law that considers the physical processes involved has been proposed. Based on the assumption that the sliding of one clay particle over another obeys the activation energy concept, rate process theory has been adopted to study the creep behavior of clays (2,7,10). However, cases considered to date involve the assumptions that the material is isotropic and the interparticle shear forces that produce sliding are all equal and proportional to the macroscopic shear stress, the latter of which is not true in reality.

The objective of this study is to develop a refined model for the multiaxial creep of clay in which these simplifying assumptions are obviated. In addition to giving an improved formulation for the stress dependence of the creep rate, such a model will allow the anisotropy of the clay fabric to be taken into account. The mathematical model then is applied to the analysis of data from creep tests on isotropic and anisotropic specimens of a kaolin clay. Cylindrical test specimens with their longitudinal axes in mutually orthogonal directions have been trimmed from laboratory consolidated blocks of clay (8) and incremental creep tests have been conducted under conditions of constant stress and constant temperature. The distributions of particle orientations for the test specimens

Note.—Discussion open until July 1, 1975. To extend the closing date one month, a written request must be filed with the Editor of Technical Publications, ASCE. This paper is part of the copyrighted Journal of the Engineering Mechanics Division, Proceedings of the American Society of Civil Engineers, Vol. 101, No. EM1, February, 1975. Manuscript was submitted for review for possible publication on January 7, 1974.

[1]Prof. of Civ. Engrg., Northwestern Univ., Evanston, Ill.

[2]Staff Engr., Dames and Moore, Park Ridge, Ill.; formerly, Grad. Research Asst., Dept. of Civ. Engrg., Northwestern Univ., Evanston, Ill.

[3]Prof. of Civ. Engrg., Northwestern Univ., Evanston, Ill.

have been determined by use of x-ray diffractometry and appropriate statistical formulations have been incorporated into the mathematical model, which is limited to creep at constant stress.

IDEALIZATION OF MICROSTRUCTURE AND KINEMATICS OF TRIANGULAR CELL

Many clay soils are comprised of microscopic platelets that may be arranged in a large variety of geometrical configurations, termed the fabric of the clay. The so-called cardhouse arrangement, illustrated in Fig. 1(*a*), is one of the most commonly assumed configurations and has been substantiated in many instances by scanning electron micrographs. Clay fabric, together with the forces acting between particles, constitute the structure of the clay, and clay structure at the microscale governs the mechanical behavior of the clay at the macroscale. However, the exact nature of these interparticle bonds is largely unknown and virtually impossible to quantify. This represents the greatest single shortcoming in the development of realistic models of the microstructure. Nevertheless, despite this inadequate knowledge regarding bonding mechanisms and their relationship to fabric and pore fluid chemistry, it may be assumed reasonably that the forming and breaking of bonds is governed by rate process theory.

The contact area between two adjacent particles is relatively small and it is likely that adsorbed water on the particle surfaces and the cations in the pore fluid participate strongly in the contact structure. An interparticle contact may contain many bonds and complete failure in shear involves the simultaneous failure of all bonds associated with all particle contacts along the shear plane. At subfailure stresses, creep is likely to be caused by the sliding of one particle relative to another due to a sequence of breaking and forming interparticle bonds. Accordingly, the clay fabric (particle spacing and orientation) and the pore fluid chemistry, both of which affect the interparticle distances at the contact zones, and the thicknesses of the adsorbed water layers should have a definite effect on the rate of bond failures. To make the problem tractable, the following simplifying assumptions will be made.

Assumption 1.—The clay fabric is considered to be a two-dimensional array of individual particles, as shown in Fig. 1(*b*), and the three-dimensional formulation can be synthesized approximately from the two-dimensional one.

Assumption 2.—Most particles have negligible thickness relative to their length and are plate-like rather than sheet-like or rod-like.

Assumption 3.—For a constant macroscopic load, the particles are in a time-constant stress state, so that changes in the elastic deformation of the particles are negligible. In other words, the particles can be treated as perfectly rigid.

Assumption 4.—Creep consists in the sliding of the edge of one particle over the face of an adjacent particle.

Assumption 5.—The macroscopic load is carried solely by statically determinate triangular cells, shown in Figs. 2(*a*) and 2(*b*), formed by three particles, each of which has only one edge touching another particle of the cell.

Assumption 6.—The displacements in the macroscopic continuum match the average of the displacements of the particle edges in the cells, the average being taken over a large number of cells.

Assumption 5 excludes polygons with more than three sides [case 2 in Fig. 2(*c*)] and many other configurations [Fig. 2(*c*)] that are not easily amenable to analysis. Those that are kinematically indeterminate [cases 2 and 3, Fig. 2(*c*)] cannot by themselves resist the applied load. The statically indeterminate configurations, e.g., those shown in cases 4, 5, and 6 of Fig. 2(*c*), can carry

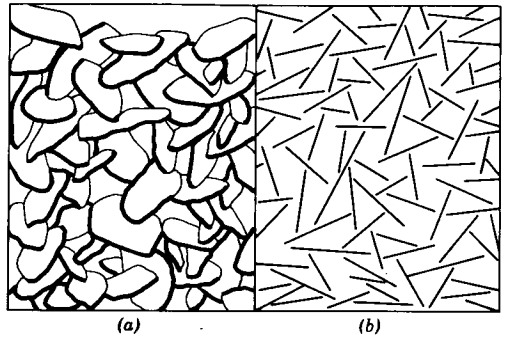

FIG. 1.—Clay Microstructure: (*a*) Schematic (14); (*b*) Associated Two-Dimensional Idealization

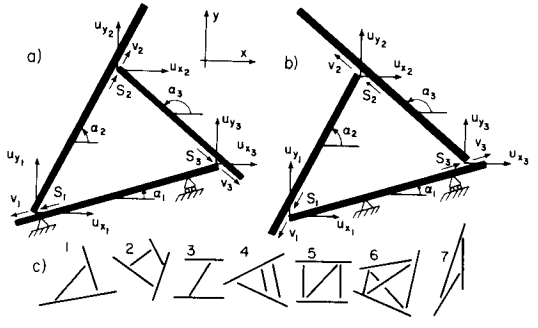

FIG. 2.—Basic Triangular Cell and Other Possible Configurations

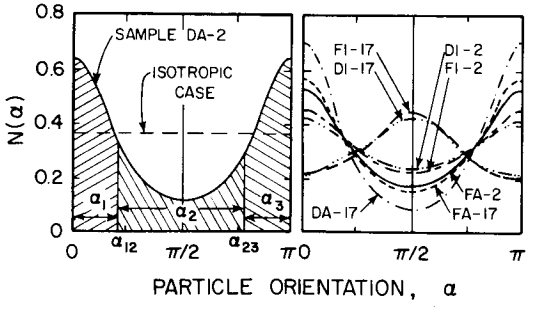

FIG. 3.—Planar Projections of Particle Orientation Density Distributions

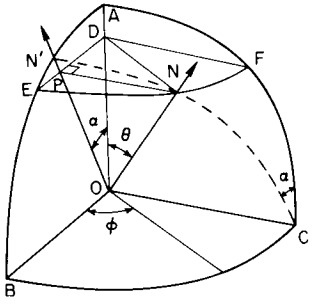

FIG. 4.—Projection of Normal to Clay Particle on Plane

the applied load, but these configurations probably have a much smaller frequency of occurrence because they are geometrically overdeterminate. Statical indeterminacy also may arise when a moment can be transmitted at particle tips; this moment is herein assumed to be negligible. With regard to assumption 4, note that apart from sliding, particles also can approach each other, but this mode of deformation results mainly in consolidation rather than creep.

As a more general and possibly more realistic model, creep may be assumed to consist essentially of the sliding of a group of particles over an adjacent group. If the arrangement of particles within each group is assumed to be fixed, the present theory is also applicable. In this case the words "particle" or "platelet" in the ensuing development must be everywhere replaced by the phrase "group of particles" or "group of platelets."

In view of assumption 6, the basic kinematic parameters of the cell are best chosen as the displacement components, u_{x_i} and u_{y_i} $(i = 1,2,3)$, of the contact edges, referred to cartesian coordinates x and y. The column matrices of displacements are

$$\mathbf{u}_i = (u_{x_i}, u_{y_i})^T; \quad \mathbf{u} = (u_{x_1}, u_{x_2}, u_{x_3}, u_{y_1}, u_{y_2}, u_{y_3})^T \quad \ldots\ldots\ldots\ldots\ldots (1)$$

in which the superscript, T, designates a transpose. Similar to constant strain triangles in the finite element method (16), the six displacement parameters in Eq. 1 for the triangular cell can be associated uniquely with a homogeneous strain field, defined as

$$\underset{\sim}{\epsilon} = (\epsilon_x, \epsilon_y, \gamma_{xy})^T = \left(\frac{\partial u_x}{\partial x}, \frac{\partial u_y}{\partial y}, \frac{\partial u_x}{\partial y} + \frac{\partial u_y}{\partial x}\right)^T \quad \ldots\ldots\ldots\ldots\ldots (2)$$

in which ϵ_x, ϵ_y, and γ_{xy} are the linearized (small) normal strains and the shear strain (shear angle), respectively, and

$$u_x = \frac{1}{2\Delta}\{[y_{32}(x - x_2) - x_{32}(y - y_2)]\, u_{x_1} + [-y_{31}(x - x_3)$$

$$+ x_{31}(y - y_3)]\, u_{x_2} + [y_{21}(x - x_1) - x_{21}(y - y_1)]\, u_{x_3}\} \quad \ldots\ldots\ldots\ldots (3a)$$

$$u_y = \frac{1}{2\Delta}\{[y_{32}(x - x_2) - x_{32}(y - y_2)]\, u_{y_1} + [-y_{31}(x - x_3)$$

$$+ x_{31}(y - y_3)]\, u_{y_2} + [y_{21}(x - x_1) - x_{21}(y - y_1)]\, u_{y_3}\} \quad \ldots\ldots\ldots\ldots (3b)$$

in which $x_{ij} = x_i - x_j$; $y_{ij} = y_i - y_j$; and Δ = area of triangle. To assure a positive value for Δ, the corners of the triangle must be numbered clockwise. Eqs. 3 are derived by assuming general linear expressions in x and y for u_x and u_y and imposing the conditions that the nodal displacements must be obtained for nodal coordinates. Substitution of Eqs. 3 into Eq. 2 yields

$$\underset{\sim}{\epsilon} = \mathbf{B}\mathbf{u} \quad \ldots\ldots\ldots\ldots\ldots (4)$$

in which $$\mathbf{B} = \frac{1}{2\Delta}\begin{bmatrix} b_1 & b_2 & b_3 & 0 & 0 & 0 \\ 0 & 0 & 0 & c_1 & c_2 & c_3 \\ c_1 & c_2 & c_3 & b_1 & b_2 & b_3 \end{bmatrix} \quad \ldots\ldots\ldots\ldots\ldots (5)$$

and $b_i = y_k - y_j$; and $c_i = x_j - x_k$ where $(i,j,k) = (1,2,3)$, $(2,3,1)$, or $(3,1,2)$. It is expedient to express b_i and c_i in terms of Δ and the direction angles, α_1, α_2, and α_3, of the particles, as defined in Fig. 2(*a*). Then, $b_1 = -b_1'$, $b_2 = -b_2'$, $b_3 = b_3'$, $c_1 = c_1'$, $c_2 = c_2'$, $c_3 = -c_3'$, and

$$b_i' = b_i'' \sin \alpha_k; \quad c_i' = b_i'' \cos \alpha_k; \quad b_i'' = \left[\frac{2\Delta \sin (\alpha_j - \alpha_i)}{\sin (\alpha_k - \alpha_i) \sin (\alpha_k - \alpha_j)} \right]^{1/2} \tag{6}$$

The edge displacement rates, $\dot{\mathbf{u}}$, of the particles in the cell uniquely determine the relative slip velocities, v_i, at the particle contacts, and one can readily find

$$\mathbf{v} = (v_1, v_2, v_3)^T = \mathbf{c}\dot{\mathbf{u}} \quad \ldots\ldots\ldots\ldots\ldots\ldots\ldots\ldots\ldots\ldots\ldots\ldots\ldots\ldots (7)$$

in which the dot denotes a time derivative ($\dot{u} = du/dt$). For the configuration shown in Fig. 2(*a*):

$$\mathbf{c} = \begin{bmatrix} -\cos\alpha_1 & 0 & \cos\alpha_1 & -\sin\alpha_1 & 0 & \sin\alpha_1 \\ -\cos\alpha_2 & \cos\alpha_2 & 0 & -\sin\alpha_2 & \sin\alpha_2 & 0 \\ 0 & \cos\alpha_3 & -\cos\alpha_3 & 0 & \sin\alpha_3 & -\sin\alpha_3 \end{bmatrix} \quad \ldots\ldots (8a)$$

and, for the configuration shown in Fig. 2(*b*):

$$\mathbf{c} = \begin{bmatrix} -\cos\alpha_2 & \cos\alpha_2 & 0 & -\sin\alpha_2 & \sin\alpha_2 & 0 \\ 0 & \cos\alpha_3 & -\cos\alpha_3 & 0 & \sin\alpha_3 & -\sin\alpha_3 \\ -\cos\alpha_1 & 0 & \cos\alpha_1 & -\sin\alpha_1 & 0 & \sin\alpha_1 \end{bmatrix} \quad \ldots\ldots (8b)$$

Furthermore, it is necessary to express the slip velocities, $\mathbf{v}$, in terms of the macroscopic strain rates, $\dot{\epsilon}$. These cannot be obtained by inverting matrix $\mathbf{B}$ in Eq. 4 because $\mathbf{B}$ is not a square matrix. This is due to the fact that $\mathbf{u}$ may include rigid body rotations, which are immaterial for stress-strain relations because no work is done by the stresses. Thus, without sacrificing generality, one may introduce an arbitrary statically determinate support for the basic cell. It can be verified that the resulting expressions (Eqs. 26 and 27) are the same for any such support. The support will be introduced for particle 1 in Fig. 2(*a*) or Fig. 2(*b*). Under this assumption one obtains

$$\dot{u}_{y1}, \dot{u}_{y2}, \dot{u}_{y3})^T = \underset{\sim}{\beta}(\dot{u}_{x_1}, \dot{u}_{x_2}, \dot{u}_{x_3})^T; \quad \underset{\sim}{\epsilon} = \underset{\sim}{\gamma}(\dot{u}_{x_1}, \dot{u}_{x_2}, \dot{u}_{x_3})^T \quad \ldots\ldots\ldots (9)$$

in which

$$\underset{\sim}{\beta} = [\beta_{ij}] = \begin{bmatrix} \tan\alpha_1 & 0 & 0 \\ 0 & -\cot\alpha_3 & -\cot\alpha_3 - \tan\alpha_3 \\ 0 & 0 & \tan\alpha_3 \end{bmatrix}$$

$$\text{or} \quad \underset{\sim}{\beta} = [\beta_{ij}] = \begin{bmatrix} \tan\alpha_2 & 0 & 0 \\ -\cot\alpha_2 - \tan\alpha_2 & -\cot\alpha_2 & 0 \\ 0 & 0 & \tan\alpha_1 \end{bmatrix} \quad \ldots\ldots\ldots (10)$$

and

$$\underset{\sim}{\gamma} = \begin{bmatrix} b_1 & b_2 & b_3 \\ \beta_1' & \beta_2' & \beta_3' \\ \beta_1'' & \beta_2'' & \beta_3'' \end{bmatrix}; \quad \beta_i' = \sum_{k=1}^{3} c_k \beta_{ki}; \quad \beta_i'' = c_i + \sum_{k=1}^{3} b_k \beta_{ki} \quad \ldots\ldots\ldots (11)$$

From Eqs. 7 and 9, it follows that

$$\dot{\mathbf{u}} = \mathbf{b}\underset{\sim}{\dot{\epsilon}}; \quad \mathbf{v} = \mathbf{c}\mathbf{b}\underset{\sim}{\dot{\epsilon}}; \quad \text{with} \quad \mathbf{b} = \begin{Bmatrix} \underset{\sim}{\gamma}^{-1} \\ \underset{\sim}{\beta}\,\underset{\sim}{\gamma}^{-1} \end{Bmatrix} \quad \ldots\ldots\ldots\ldots\ldots\ldots\ldots (12)$$

Use of the support condition for particle 1 allows Eq. 7 to be reduced to

$$\mathbf{v} = \underset{\sim}{\alpha}(\dot{u}_{x_1}, \dot{u}_{x_2}, \dot{u}_{x_3})^T \quad \ldots\ldots\ldots\ldots\ldots\ldots\ldots\ldots\ldots\ldots\ldots (13)$$

in which $\underset{\sim}{\alpha}$ is expressed in terms of $\mathbf{c}$ and $\underset{\sim}{\beta}$ in the same manner as $\underset{\sim}{\gamma}$ is expressed in terms of $\mathbf{b}$ and $\underset{\sim}{\beta}$. Then

$$\dot{\mathbf{u}} = \mathbf{D}\mathbf{v}; \quad \underset{\sim}{\dot{\epsilon}} = \mathbf{B}\mathbf{D}\mathbf{v}; \quad \text{with} \quad \mathbf{D} = \begin{Bmatrix} \underset{\sim}{\alpha}^{-1} \\ \underset{\sim}{\beta}\,\underset{\sim}{\alpha}^{-1} \end{Bmatrix} \quad \ldots\ldots\ldots\ldots\ldots\ldots (14)$$

Correlation of Microscopic and Macroscopic Creep Laws through Energy Dissipation

According to rate process theory (2,3,7,10), the relative slip velocity, v_i, and the tangential force, S_i, at the ith interparticle contact ($i = 1,2,3$; Fig. 2) may be related by

$$v_i = k_1 \sinh(k_2 S_i); \quad \text{with} \quad k_1 = 2X\frac{kT}{h}\exp\left(-\frac{\Delta F}{RT}\right) \quad \text{and} \quad k_2 = \frac{\lambda}{2kT} \tag{15}$$

in which k_1 and k_2 are material parameters (of which k_1 is a given function of time, provided S_i is time-constant); T = absolute temperature; ΔF = activation energy of creep; k = Boltzmann's constant; h = Planck's constant; R = universal gas constant; λ = distance between successive equilibrium positions of the broken and reformed bond; and X = parameter that depends on λ and the number of bonds in the contact area.

For a wide range of clay soils and stress levels, Singh and Mitchell (13) showed that the time-dependence is described adequately by the power law, $\dot{\epsilon} = c(t_1/t)^m$, in which m, c, and t_1 are constants that can be determined readily from logarithmic time plots. If rate process theory is adopted for the stress dependence of creep (at constant load), this result suggests that

$$k_1 = k_0 t^{-m} \quad \ldots\ldots\ldots\ldots\ldots\ldots\ldots\ldots\ldots\ldots\ldots\ldots\ldots\ldots (16)$$

in which m and k_0 = constants (k_0 = the value of k at unit time). The constant, m, characterizes the time dependence of creep in soils; usually, $0.7 \leq m \leq 1$. It will be shown that the experiments reported herein conform reasonably well to this power law.

It will be helpful to carry out an incremental (tangential) linearization of Eq. 15, which is nonlinear. Using the first two terms of a Taylor series expansion about point (S_i, v_i), one gets

$$\bar{v}_i = k_1 \sinh(k_2 S_i) + k_1 k_2 \cosh(k_2 S_i)(\bar{S}_i - S_i) \quad \ldots\ldots\ldots\ldots\ldots (17)$$

in which the bar is used to label the quantities of a linearized relationship. No error is introduced by this procedure because only points $(\bar{S}_i, \bar{v}_i)$ that are infinitesimally close to (S_i, v_i) will be considered. Rewriting Eq. 17, one obtains

$$\bar{\mathbf{S}} = \mathbf{A}\bar{\mathbf{v}} + \mathbf{S}^0 \quad \text{with} \quad \bar{\mathbf{S}} = (\bar{S}_1, \bar{S}_2, \bar{S}_3)^T \quad \text{and} \quad \mathbf{S}^0 = (S_1^0, S_2^0, S_3^0)^T \quad \ldots\ldots (18)$$

in which

$$\mathbf{A} = [A_{ij}]; \quad A_{ij} = \frac{\delta_{ij}}{k_1 k_2 \cosh(k_2 S_i)}; \quad S_i^0 = S_i - v_i A_{ii}$$

$$= S_i - \frac{\tanh(k_2 S_i)}{k_2} \quad \ldots\ldots (19)$$

and δ_{ij} = Kronecker delta. The macroscopic multiaxial stress-strain relations for creep under constant stress also can be written in linearized form as

$$\bar{\underset{\sim}{\sigma}} = \underset{\sim}{\eta}(\dot{\bar{\underset{\sim}{\epsilon}}} - \dot{\underset{\sim}{\epsilon}}^0) = \underset{\sim}{\eta}\,\dot{\bar{\underset{\sim}{\epsilon}}} + \underset{\sim}{\sigma}^0 \quad \ldots\ldots (20)$$

with $\bar{\underset{\sim}{\sigma}} = (\bar{\sigma}_x, \bar{\sigma}_y, \bar{\tau}_{xy})^T$; $\dot{\underset{\sim}{\epsilon}}^0 = (\dot{\epsilon}_x^0, \dot{\epsilon}_y^0, \dot{\gamma}_{xy}^0)^T$;

$$\underset{\sim}{\sigma}^0 = (\sigma_x^0, \sigma_y^0, \tau_{xy}^0)^T = -\underset{\sim}{\eta}\,\dot{\underset{\sim}{\epsilon}}^0 \quad \ldots\ldots (21)$$

in which η = incremental (tangential) viscosity matrix (of size 3 × 3); $\dot{\underset{\sim}{\epsilon}}^0$ = nonviscous (or inviscid) strain rate; and σ^0 = nonviscous (or inviscid) stress. The $\underset{\sim}{\sigma}$—$\dot{\underset{\sim}{\epsilon}}$ relations are, of course, nonlinear, and therefore $\underset{\sim}{\eta}$, $\dot{\underset{\sim}{\epsilon}}^0$, and $\underset{\sim}{\sigma}^0$ are all functions of $\underset{\sim}{\sigma}$ (or $\dot{\underset{\sim}{\epsilon}}$). However, it is important to realize that for infinitesimal deviations of state $(\bar{\underset{\sim}{\sigma}}, \dot{\bar{\underset{\sim}{\epsilon}}})$ from the tangent point $(\underset{\sim}{\sigma}, \dot{\underset{\sim}{\epsilon}})$, no error is incurred.

The preceding linearizations are crucial steps in correlating the macroscopic and microscopic behavior. The situation is analogous to the use of linearized incremental stress-strain relations in elasto-plasticity; $\underset{\sim}{\eta}$, $\dot{\underset{\sim}{\epsilon}}^0$, and $\underset{\sim}{\sigma}^0$ are analogous to the incremental (tangential) elastic moduli, the inelastic strains, and the inelastic stresses, respectively.

The energy dissipation rate, $\mathscr{D}$, within the triangular cell can be expressed in terms of either macroscopic parameters or microscopic parameters, and both expressions must be equal, yielding

$$\mathscr{D} = \bar{\underset{\sim}{\sigma}}^T \dot{\bar{\underset{\sim}{\epsilon}}} \Delta = k_c \bar{\mathbf{S}}^T \bar{\mathbf{v}} \quad \ldots\ldots (22)$$

in which $k_c = k_c' k_c''$; and $k_c' = 1/2$ when there is a statically determinate triangle on each side of the particle (i.e., the particle belongs to two cells) and $k_c' = 1$ when there is a statically determinate triangle on one side and a kinematically indeterminate figure [e.g., cell 2 from Fig. 2(*c*)] on the other side (i.e., the particle belongs to only one cell). As an average for many cells, $1/2 < k_c < 1$. Coefficient k_c'' is the fraction of a macroscopic unit area in the material that is occupied by triangular cells; $k_c'' < 1$, perhaps $k_c'' \approx 1/2$. Note that $\Delta/k_c = 3n/N$; in which N = the number of bonds per unit macroscopic area; and n = the number of bonds per edge. Substitution of Eq. 14 for $\dot{\bar{\underset{\sim}{\epsilon}}}$ and of Eqs. 20, 18, and 12 for $\bar{\underset{\sim}{\sigma}}$, $\bar{\mathbf{S}}$, and $\bar{\mathbf{v}}$, respectively, into Eq. 22 yields

$$\bar{\underset{\sim}{\sigma}}^T \mathbf{B}\mathbf{D}\bar{\mathbf{v}}\Delta = k_c \bar{\mathbf{S}}^T \bar{\mathbf{v}} \quad \ldots\ldots (23)$$

$$\dot{\underset{\sim}{\epsilon}}^T \underset{\sim}{\eta}\,\dot{\underset{\sim}{\epsilon}} + \underset{\sim}{\sigma}^{0T}\dot{\underset{\sim}{\epsilon}} = \dot{\underset{\sim}{\epsilon}}^T \frac{k_c}{\Delta}\mathbf{b}^T\mathbf{c}^T\mathbf{A}\mathbf{c}\mathbf{b}\,\dot{\underset{\sim}{\epsilon}} + \frac{k_c}{\Delta}\mathbf{S}^{0T}\mathbf{c}\mathbf{b}\,\dot{\underset{\sim}{\epsilon}} \quad \ldots\ldots (24)$$

These two equations must be satisfied for any column matrices $\dot{\underset{\sim}{\epsilon}}$ and $\bar{\mathbf{v}}$ that are infinitesimally close to $\dot{\underset{\sim}{\epsilon}}$ and $\mathbf{v}$. Recalling the basic lemma of variational calculus, Eq. 24 is fulfilled for any $\dot{\underset{\sim}{\epsilon}}$ if, and only if

$$\dot{\underset{\sim}{\epsilon}}^T \underset{\sim}{\eta} + \underset{\sim}{\sigma}^{0T} = \dot{\underset{\sim}{\epsilon}}^T \frac{k_c}{\Delta}\mathbf{b}^T\mathbf{c}^T\mathbf{A}\mathbf{c}\mathbf{b} + \frac{k_c}{\Delta}\mathbf{S}^{0T}\mathbf{c}\mathbf{b} \quad \ldots\ldots (25)$$

Applying the same consideration again with regard to $\dot{\underset{\sim}{\epsilon}}^T$ and $\mathbf{v}$ in Eqs. 25 and 23, one reaches the following result:

$$\mathbf{S} = \frac{\Delta}{k_c}\mathbf{D}^T\mathbf{B}^T\underset{\sim}{\sigma} \quad \ldots\ldots (26)$$

$$\underset{\sim}{\eta} = \frac{k_c}{\Delta}\mathbf{b}^T\mathbf{c}^T\mathbf{A}\mathbf{c}\mathbf{b}; \quad \underset{\sim}{\sigma}^0 = \frac{k_c}{\Delta}\mathbf{b}^T\mathbf{c}^T\mathbf{S}^0 \quad \ldots\ldots (27)$$

Note that both η and $\underset{\sim}{\sigma}^0$ depend on $\underset{\sim}{\sigma}$, because $\mathbf{A}$ and $\mathbf{S}^0$ in Eq. 27 are both functions of $\bar{\mathbf{S}}$, which is, in turn, a function of $\underset{\sim}{\sigma}$, defined by Eq. 26. Given the macroscopic stress level and the geometry of the triangular cell, one may compute $\mathbf{S}$ from Eq. 26 and, subsequently, $\underset{\sim}{\eta}$ and $\underset{\sim}{\sigma}^0$ from Eq. 27. The results are exact within the limitations of the assumptions specified.

Statistical Aspects of Clay Microstructure

Eqs. 26 and 27 would apply only if all triangular cells were identical. In reality, the particle orientations, α_1, α_2, and α_3, and the cell area, Δ, are random variables with certain statistical distributions. The orientation distributions of the three particles of each cell are certainly not independent, but correlated, so that one should speak of joint probability densities. For example, if particle 1 with a given orientation α_1 is specified, orientation α_2 of particle 2 is unlikely to be close to α_1. One reason probably is that the total surface Gibbs free energy for the solid walls of a rounded void is less than that for an elongated void of equal volume. This type of correlation between the orientation probabilities will be considered herein by dividing the region $(0,\pi)$ of $N(\alpha)$, the probability density distribution of orientation α for all particles (Fig. 3), into three subregions with equal areas, i.e., $(0,\alpha_{12})$, $(\alpha_{12},\alpha_{13})$, and (α_{13},π), and by assuming that each of the orientations, α_1, α_2, and α_3, of the sides of a cell lies only within one respective subregion. This assumption obviously reduces the frequency of occurrence of cells with very small angles. In fact, such a case can occur only when α is very close to 0, α_{12}, α_{23}, or π. There is, obviously, a certain bias for angles 0, α_{12}, α_{23}, but it is insignificant because subregions $(\beta,\alpha_{12}+\beta)$, $(\alpha_{12}+\beta,\alpha_{23}+\beta)$, and $(\alpha_{23}+\beta,\pi+\beta)$ with any value of β yielded the same results in practical computations. Thus, averaging with regard to β appeared to be unnecessary. The introduction of subregions also involves another simplification because it excludes triangles [e.g., case 7 in Fig. 2(*c*)] in which the orientation of two or three sides falls within one region in Fig. 3. Nevertheless, this assumption is not considered to be excessively restrictive, because the frequency of such cases is probably quite small.

The probability density distribution, $p(\Delta)$, for the areas, Δ, of the triangular cells can be obtained from the cumulative experimental distribution functions

for pore sizes, which have been obtained by mercury intrusion tests (4). According to these data a plot of the cumulative volume (or area, in the two-dimensional case) of pores versus the logarithm of the volume (or area) of individual pores is approximately a straight line. Thus

$$p(\Delta) = \frac{\Delta_1 \Delta_2}{\Delta_2 - \Delta_1} \frac{1}{\Delta^2} \quad \ldots\ldots\ldots\ldots\ldots\ldots\ldots\ldots\ldots\ldots \quad (28)$$

in which Δ_1 and Δ_2 = the smallest and the largest values of Δ in the material. Values of 2×10^{-11} cm^2 and 10^{-8} cm^2 for Δ_1 and Δ_2, respectively, were used in all computations reported herein.

Assuming that the interparticle forces, **S**, for all cells of different shape correspond to the same macroscopic stress state, $\underset{\sim}{\sigma}$, one may obtain the averaged macroscopic incremental viscosities and nonviscous stresses as

$$\underset{\sim}{\eta} = \int_{\Delta_1}^{\Delta_2} \int_{\alpha_{23}}^{\pi} \int_{\alpha_{12}}^{\alpha_{23}} \int_{0}^{\alpha_{12}} \mathbf{f}(\alpha_1, \alpha_2, \alpha_3, \Delta)\, N(\alpha_1)\, N(\alpha_2)\, N(\alpha_3)\, p(\Delta)\, d\alpha_1\, d\alpha_2\, d\alpha_3\, d\Delta \quad (29a)$$

$$\underset{\sim}{\sigma}^0 = \int_{\Delta_1}^{\Delta_2} \int_{\alpha_{23}}^{\pi} \int_{\alpha_{12}}^{\alpha_{23}} \int_{0}^{\alpha_{12}} \mathbf{g}(\alpha_1, \alpha_2, \alpha_3, \Delta)\, N(\alpha_1)\, N(\alpha_2)\, N(\alpha_3)\, p(\Delta)\, d\alpha_1\, d\alpha_2\, d\alpha_3\, d\Delta \quad (29b)$$

$$\text{in which} \quad \mathbf{f} = [(\underset{\sim}{\eta})_a + (\underset{\sim}{\eta})_b]/2; \quad \mathbf{g} = [(\underset{\sim}{\sigma}^0)_a + (\underset{\sim}{\sigma}^0)_b]/2 \quad \ldots\ldots\ldots \quad (30)$$

Here, $\underset{\sim}{\eta}$ and $\underset{\sim}{\sigma}^0$ are evaluated from Eqs. 26 and 27 for the kinds of cell configurations designated by subscripts a and b, respectively, as shown in Figs. 2(a) and 2(b). To satisfy the conditions of symmetry of the material, both kinds of configurations must occur with equal frequency within a sufficiently large volume. Therefore, Eq. 30 introduces the average of the values obtained for the configurations shown in Figs. 2(a) and 2(b).

The assumptions regarding statistics may be checked easily in the case of an isotropic material, for which $N(\alpha)$ is a constant (which corresponds to a perfectly random orientation of particles). Components η_{ij} of matrix $\underset{\sim}{\eta}$ must then satisfy the conditions, $\eta_{13} = \eta_{31} = \eta_{23} = \eta_{32} = 0$; $\eta_{22} = \eta_{11}$; $\eta_{12}/\eta_{11} = \eta_{21}/\eta_{11} = \nu'$; and $\eta_{33} = \eta_{11}(1 - \nu')/2$. Computer calculations indicated that these conditions are indeed satisfied, with an error of not more than 0.1%. Thus, the statistical assumptions regarding particle orientations appear to be acceptable. These calculations always yield a value of 1/3 for Poisson's ratio in creep, ν'. This is not surprising because it is known that the microstructure of an isotropic elastic material idealized as any isotropic system of elastic bars always leads to a Poisson's ratio of 1/3 (9) if no constraint to constant-volume is imposed. However, when the three-dimensional case and the constant-volume constraint are considered in the next section, the correct value of $\nu' = 1/2$ is assured.

For an $N(\alpha)$ distribution that is symmetric about $\pi/2$, the material is transversely isotropic (in three dimensions). By imposing the condition that the x-axis must coincide with the direction, $\alpha = \pi/2$, one must obtain $\eta_{13} = \eta_{23} = \eta_{31} = \eta_{32} = 0$, and for $\tau_{xy} = 0$ one must get $\tau^0_{xy} = 0$. These conditions also were found to be satisfied with an error of less than 0.1%. Moreover, computations

always yielded nearly exactly equal values of η_{12} and η_{21}. This means that η_{ij} values are derivable by double differentiation from a certain scalar potential (dissipation potential). In fact, one could prove that this must be so, because v_i does not depend on any force that would do no work, such as the normal force in the contact of particles.

Experimental data characterizing the distribution of particle orientations were obtained from x-ray diffraction tests that were performed on carbowax impregnated thin sections (approx 100 μ thick) according to the method developed by Baker, Wenk, and Christie (1) and Tullis (15). Fabric effects were averaged over an area approximately 1 mm in diameter, and the results were plotted in the form of polar orientation density distributions, $n(\theta,\phi)$, in which θ and ϕ = the spherical coordinates of the normal to the clay platelet. Once axial symmetry had been ascertained (all samples were either isotropic or cross-anisotropic), $n(\theta,\phi)$ reduces to $n(\theta)$, which may be converted into the planar orientation density distribution, $N(\alpha)$, in which α is measured from the axis of symmetry, by projecting the normals of clay platelets onto a plane containing the axis of symmetry and normalizing the result with respect to the total intensity, N_T. The geometry associated with this projection is shown in Fig. 4. The number of particles having a projected normal with an angle equal to or greater than α is

$$N^*(\alpha) = \int_0^{\pi/2} \left(\int_{f(\alpha,\phi)}^{\pi/2} n(\theta) \sin\theta\, d\theta \right) d\phi \quad \ldots\ldots\ldots\ldots\ldots\ldots \quad (31)$$

in which $f(\alpha,\phi) = \arctan(\tan\alpha/\cos\phi)$ because $\tan\alpha = (\sin\theta\cos\phi)/\cos\theta$ and $\tan\theta = \tan\alpha/\cos\phi$. Due to symmetry, integration is necessary only over the first octant. Since $N^*(\alpha)$ is the cumulative distribution, the projected planar orientation density distribution (Fig. 3) is

$$N(\alpha) = \frac{1}{N_T} \frac{dN^*(\alpha)}{d\alpha} = -\frac{1}{N_T} \int_0^{\pi/2} \frac{df(\alpha,\phi)}{d\alpha}\, n[f(\alpha,\phi)] \sin[f(\alpha,\phi)]\, d\phi \quad (32)$$

in which constant N_T is determined from the normalizing condition, $\int_0^{\pi} N(\alpha)d\alpha = 1$ or $2N^*(0) = 1$, which, after substitution for N^* from Eq. 31, yields $N_T = \pi \int_0^{\pi/2} n(\theta) \sin\theta\, d\theta$. In the plane case, the particle orientations are defined by angles α_i of the particle rather than their normals (Fig. 2), and the conversion from α to α_i is accomplished by substituting $\alpha = \alpha_i \pm \pi/2$.

Approximate Generalizations to Three Dimensions

The anisotropic microstructure of clays is produced in large part by the anisotropy of the stress state under which it is consolidated. The axis of the maximum principal stress during consolidation will be identified as the x-axis. This area is normal to the prevalent orientation of clay platelets. In the laboratory consolidation techniques employed, the stress state during consolidation is axisymmetric about the x-axis and symmetric about the (yz)-plane, and the same must therefore be true of the microstructure produced by the consolidation process. Accordingly, it is logical to expect that the stress-strain relations of

these clay samples are transversely isotropic, provided that the stress state, $\underset{\sim}{\sigma}$, causing creep is likewise transversely isotropic, since the incremental material properties depend on $\underset{\sim}{\sigma}$.

In the three-dimensional case, stress-strain relations in the form of Eq. 20 still may be considered, but all matrices must be expanded to either (6 × 1) or (6 × 6) in size. A three-dimensional model for the determination of material parameters perhaps could be based on a mixture of tetrahedral cells and prismatic (hexahedral) cells, but such a model would be much more complicated than the two-dimensional model developed herein. In view of the other assumptions involved, such a complexity seems to be unjustified at this time, and three-dimensional situations are better treated approximately by considering projections of the microstructure on various planes, as has been done already in connection with Eq. 32. If one considers separately the (xy)-plane, the projected orientation distribution, $N(\alpha)$, within this plane (Eq. 32), and the stress state, σ_x, σ_y, and τ_{xy}, within this plane, it is possible to compute components η_{11}, η_{12}, η_{22}, η_{13}, η_{23}, and η_{33} of matrix $\underset{\sim}{\eta}$ and components σ_x^0, σ_y^0, and τ_{xy}^0 of matrix $\underset{\sim}{\sigma}^0$ from Eqs. 26 and 27. Then, the same can be repeated for the (yz) and (zx)-planes. This procedure yields the complete matrix, $\underset{\sim}{\sigma}^0$, and all coefficients of the (6 × 6) matrix $\underset{\sim}{\eta}$, except η_{15}, η_{26}, η_{34}, η_{45}, η_{46}, and η_{56}, i.e., the coefficients relating σ_x to $\dot{\gamma}_{yz}$, σ_y to $\dot{\gamma}_{xz}$, σ_z to $\dot{\gamma}_{xz}$, τ_{xy} to $\dot{\gamma}_{yz}$ and $\dot{\gamma}_{xz}$, and τ_{yz} to $\dot{\gamma}_{zx}$. These coefficients, of course, cannot be determined from planar models and must be assumed to vanish in the present study.

The coefficient, η_{11}, is obtained from computations for the (xy)-plane and then again from computations for the (yz)-plane. The results of both computations need not be the same, unless the orientation distributions, $N(\alpha)$, for each of the two planes are normalized with regard to the same number of particles. Thus, all $\underset{\sim}{\eta}$ components and $\underset{\sim}{\sigma}$ components for one of the planes [e.g., the (yz)-plane] must be proportionately adjusted to obtain the same value of η_{11} as determined from the (xy)-plane. Subsequently, the coefficient, η_{22}, is obtained from the (xy) and (yz)-planes, and now all $\underset{\sim}{\eta}$ and $\underset{\sim}{\sigma}$ components from the (yz)-plane must be proportionately adjusted to yield the same value of η_{22} as determined from the (xy)-plane. Finally, the coefficient, η_{33}, is obtained from the (xz) and (yz)-planes; however, this time both the (xz)-plane and the (yz)-plane already have been adjusted with regard to (xy), and no further proportional adjustment is justified. However, a difference in η_{33} may still appear because of the numerical error associated with the approximate nature of the three-dimensional generalization. In such a case, it is probably best to take for η_{33} the average value from both planes. Furthermore, the coefficient, σ_x^0, is also obtained twice, once from the (xy)-plane and once from the (xz)-plane; if the two values differ, their average should be taken again. The same argument applies for σ_y^0 and σ_z^0.

The axial direction of the creep specimens tested will be denoted by x' and y', and z' will identify the remaining two cartesian axes of the test specimen. To fit the test data, the stress-strain law given by Eq. 20 must be transformed (Fig. 5) from the material axes, $x_i = (x, y, z)$, to the specimen axes, $x_i' = (x', y', z')$. The transformation of the stress tensor, σ_{ij}, is expressed in tensor notation as $\sigma_{km}' = (\partial x_k'/\partial x_j)(\partial x_m'/\partial x_i)\sigma_{ij}$, which, in matrix notation, can be rewritten as $\underset{\sim}{\sigma}' = \underset{\sim}{\lambda}^T\underset{\sim}{\sigma}$, in which $\underset{\sim}{\lambda}^T$ is a (6 × 6) transformation matrix. The transformed version of Eq. 20 then becomes

TABLE 1.—Characteristics and Creep Parameters

Sample designation[a] (1)	Maximum effective consolidation stress, in N/mm² (2)	Water content of slurry, as a percentage (3)	Water content after consolidation, as a percentage (4)
DA-2	0.226[b]	249	53
DA-17	1.716[b]	260	43
FA-2	0.226[b]	251	58
FA-17	1.716[b]	253	48
DI-2	0.226[c]	247	54
DI-17	1.716[c]	249	41
FI-2	0.226[c]	261	64
FI-17	1.716[c]	271	46

[a]D = dispersed slurry with NaOH; F = flocculated slurry with $CaCl_2$; A = anisotropic
[b]Vertical.
[c]Hydrostatic.

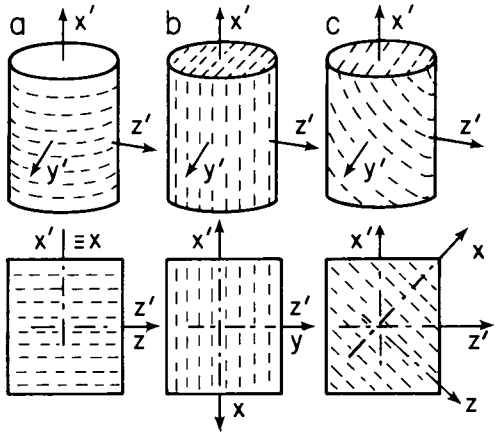

FIG. 5.—Creep Test Specimens Cut at Various Directions to Preferred Particle Orientation (Indicated by Dashed Lines)

$$\underset{\sim}{\sigma}' = (\underset{\sim}{\lambda}^T\underset{\sim}{\eta}\underset{\sim}{\lambda})\dot{\underset{\sim}{\epsilon}}' + \underset{\sim}{\lambda}^T\underset{\sim}{\sigma}^0; \quad \text{with} \quad \underset{\sim}{\sigma}' = \underset{\sim}{\lambda}^T\underset{\sim}{\sigma}; \quad \dot{\underset{\sim}{\epsilon}}' = \underset{\sim}{\lambda}^T\dot{\underset{\sim}{\epsilon}} \quad \ldots\ldots\ldots \quad (33)$$

Since the test program included only consolidated undrained creep tests for which the volume change is virtually zero, the following constraint must be introduced in the stress-strain relations:

$$\dot{\epsilon}_z = -\dot{\epsilon}_x - \dot{\epsilon}_y \quad \text{or} \quad \dot{\epsilon}_z' = -\dot{\epsilon}_x' - \dot{\epsilon}_y' \quad \ldots\ldots\ldots\ldots\ldots\ldots \quad (34)$$

Furthermore, because the hydrostatic component of the stress tensor does no

of Kaolin (Hydrite 10) Samples

Void ratio after consolidation, e (5)	Time exponent, m (6)	Stress level parameter, k_2 (N^{-1}) (7)	Creep rate parameter, k_0, mm/min. (8)
1.22	0.77	306×10^3	10.33×10^{-14}
1.08	1.00	184×10^3	17.60×10^{-14}
1.52	0.72	816×10^3	1.28×10^{-14}
1.16	0.86	235×10^3	6.27×10^{-14}
1.40	0.82	867×10^2	1.51×10^{-11}
1.16	1.00	387×10^2	4.75×10^{-11}
1.45	0.80	408×10^2	8.29×10^{-11}
1.26	0.90	204×10^2	10.20×10^{-11}

consolidation stress; I = isotropic consolidation stress.

work, it is indeterminate and unrelated to creep at constant volume. Thus, only the deviatoric component of the stress tensor may appear in the stress-strain relations. For the tests performed in this investigation, one has $\sigma'_x \neq 0$, $\sigma'_y = \sigma'_z$, and $\tau'_{xy} = \tau'_{yz} = \tau'_{zx} = 0$. Thus, the creep rate may depend only on $(\sigma'_x - \sigma'_y)$, so that Eq. 20 would simplify to the form, $\dot{\epsilon}'_x = a(\sigma'_x - \sigma'_y) + b$; in which a and b are functions of $(\sigma'_x - \sigma'_y)$.

Computer Program for Predicting Creep and Fitting Data

There are only two free parameters, k_1 and k_2, in Eq. 15 to fit the test data. Of these, k_1 = a function of time t, but if a specified time in the creep test is considered, k_1 appears to be a constant. In a computer program, which has been written to fit the creep data, the computations are performed in accordance with the following main steps:

1. Assign chosen values to k_2, m, and k_0 (Eq. 15 and Eq. 16).
2. Choose the time, t, and the stress level, σ'_x.
3. The deviatoric components of the actual stresses, σ'_x, σ'_y, and σ'_z, in the test (i.e., the components $s'_x = \sigma'_x - \sigma_v/3$, $s'_y = s'_z = -s'_x/2$, in which $\sigma_v = \sigma'_x + \sigma'_y + \sigma'_z$) are transformed to the material axes, x, y, and z (Eq. 33).
4. The (xy)-plane is considered first. For all possible combinations of chosen discrete values for α_1, α_2, α_3, and Δ, the values of $\mathbf{S}$, $\mathfrak{y}$, and $\underset{\sim}{\sigma}^0$ are evaluated (Eqs. 26 and 27) for the configurations shown in Figs. 2(a) and 2(b). Then, the statistical averaging integrals of Eq. 29 are computed by the trapezoidal rule, which yields averaged values of $\mathfrak{y}$ and $\underset{\sim}{\sigma}^0$ for the (xy)-plane.

5. Step 3 is repeated for the (xz)-plane, in which the same orientation distribution, $N(\alpha)$, applies, and then for the (yz)-plane, in which the orientation distribution is perfectly random (isotropy).
6. The elements of the two-dimensional matrices, $\mathfrak{y}$ and $\underset{\sim}{\sigma}^0$, for the (xy), (yz), and (zx)-planes are composed as described in this section to yield the three-dimensional matrices, $\mathfrak{y}$ and $\underset{\sim}{\sigma}^0$. Then, these are transformed by Eq. 33 to the x', y', and z'-axes of the test specimen.
7. Solve $\dot{\epsilon}'_x$ from Eq. 33 under the constraint specified by Eq. 34; this yields one point on the $\dot{\epsilon}'_x - \sigma'_x$ curve at constant t.
8. Repeat steps 2 through 7 for several other values of σ'_x and plot the $\dot{\epsilon}'_x - \sigma'_x$ curve. Then, repeat steps 2 through 7 to compute the curves for other times t and for other specimens (Fig. 5) of the same material.
9. Choose other values of k_2, m, and k_0 and repeat steps 1 through 8 until an acceptable fit of all data is obtained.

Experimental Investigation

All test specimens were cylindrical in shape (4 cm high with a diameter of approximately 3.5 cm) and trimmed from blocks (approximately 20 cm in diameter and 15 cm thick) of a dispersed or flocculated hydrite 10 kaolin clay that was consolidated anisotropically and isotropically from a slurry in accordance with procedures described by Sheeran and Krizek (12), Edil (5), and Krizek, Edil, and Ozaydin (8). Although no attempt was made in the sample preparation to model or duplicate the soil-making processes of nature, an effort was directed toward producing a range of fabrics that includes that of most naturally occurring sedimentary clays. Since the environmental conditions that prevail during deposition and post-depositional load history play important roles in controlling the resultant fabric of sedimentary clays, the sample preparation procedure gives considerable attention to the pore fluid chemistry of the slurry and the stress path followed during the slurry consolidation. The details of these techniques for preparing relatively large bulk samples from which test specimens were trimmed have been presented by Krizek, Edil, and Ozaydin (8).

One test specimen was trimmed vertically and one was trimmed horizontally from each anisotropically and each isotropically consolidated sample, and one specimen was trimmed with its longitudinal axis inclined at 45° to the direction of the major consolidation stress from one of the anisotropically consolidated samples (Fig. 5). All specimens were tested in undrained creep at 78° F. A constant confining stress and axial stress were maintained, and only the axial strains were measured. The basic characteristics of the samples are given in Table 1, and typical scanning electron micrographs of two samples are shown in Fig. 6. A constant axial load was maintained on each specimen for at least two days and in some cases up to seven days, during which time the axial deformations and the developed pore pressures were measured. At the end of each loading step, the load was increased to that chosen for the next step. To reduce the disturbances that usually arise when an instantaneous load is placed on an already deforming specimen, the loading arm was locked before increasing the load, the load was increased, and then the loading arm was unlocked. This was done rapidly (within a few minutes) to minimize the stress relaxation

involved. Fig. 7 shows a typical plot of strain versus time data obtained from these tests.

Observed Time-Dependence of Strain Rate.—Although the creep response of

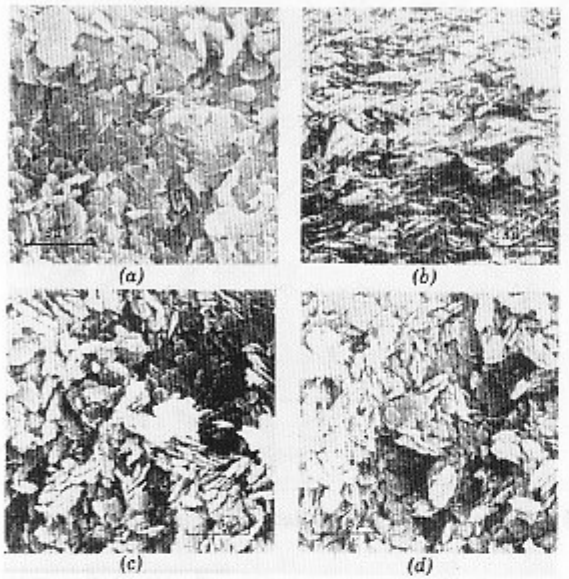

FIG. 6.—Electron Scanning Micrographs—Anisotropically Consolidated Sample from Dispersed Slurry (DA-17, Highly Anisotropic): (*a*) Horizontal Plane Normal to and (*b*) Vertical Plane Parallel to Major Principal Consolidation Stress; Isotropically Consolidated Sample from Flocculated Slurry (FI-2, Nearly Isotropic): (*c*) Plane Parallel to and (*d*) Plane Normal to General Direction of Drainage

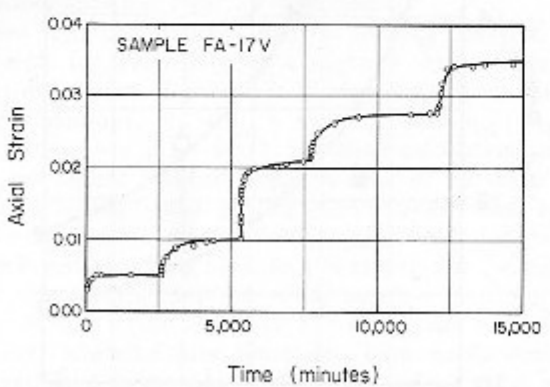

FIG. 7.—Typical Time Dependence of Strain under Step Loading (Sample FA-17)

soils under different stress levels is determined most logically by performing creep tests on a series of specimens subjected to different stresses, satisfactory results may be obtained by subjecting a single specimen to different stresses

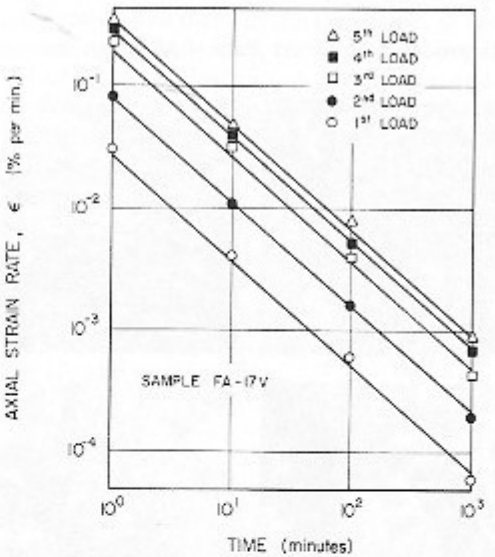

FIG. 8.—Dependence of Strain-Rate on Time under Constant Load

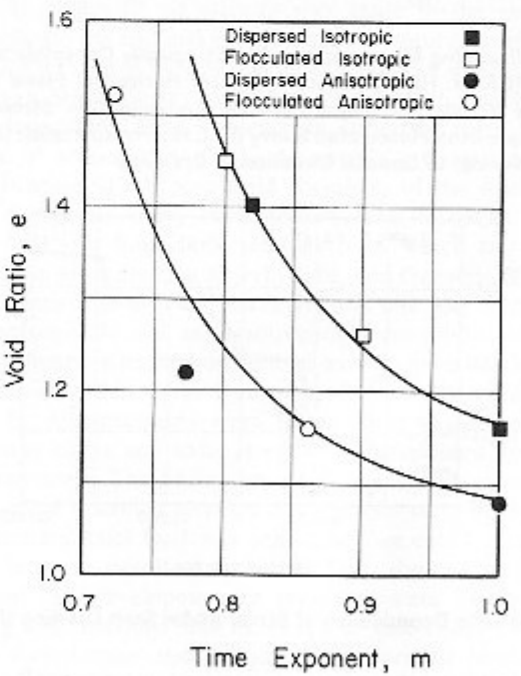

FIG. 9.—Effect of Void Ratio on Time Exponent

applied incrementally and employing the principle of superposition. In this work, the latter procedure was used due to the difficulty of producing and testing large numbers of specimens and the limitations imposed by the number of specimens that could be trimmed from the consolidated samples. Based on

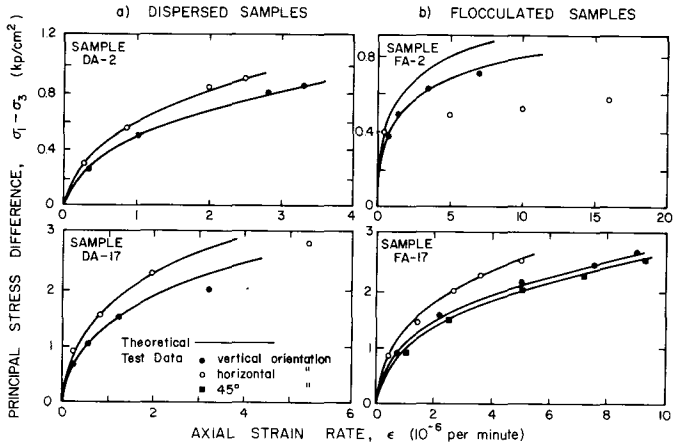

FIG. 10.—Stress Dependence of Creep Rate for Anisotropically Consolidated Samples 1,000 min after Loading (1 kp/cm² = 0.0981 N/mm²)

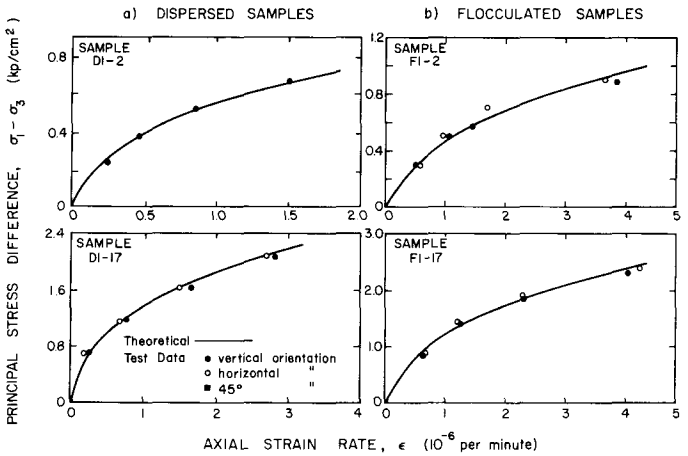

FIG. 11.—Stress Dependence of Creep Rate for Isotropically Consolidated Samples 1,000 min after Loading (1 kp/cm² = 0.0981 N/mm²)

the typical test data exemplified in Fig. 7, a representative plot of the time dependence of the axial strain rate is illustrated in Fig. 8. Values for the exponent, m, which characterizes the time-dependence of creep (Eq. 16) and results from the relationship of the shear force between two particles and the rate of relative displacement of the particles in the direction of that force, are given in Table

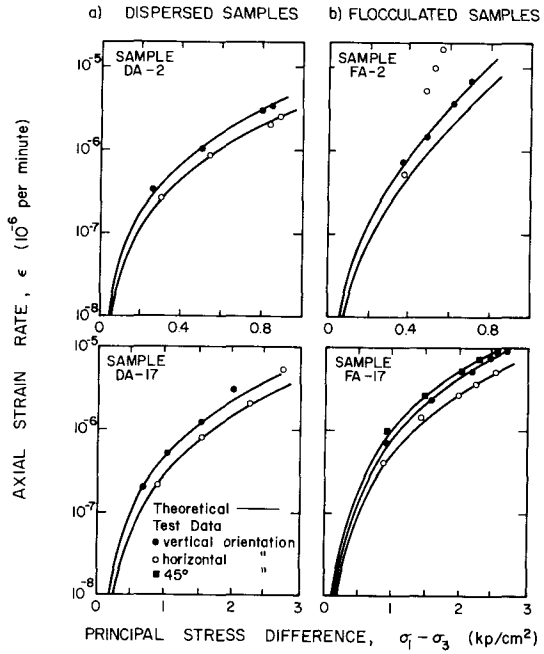

FIG. 12.—Fig. 10 Replotted in Semilog Scale (1 kp/cm² = 0.0981 N/mm²)

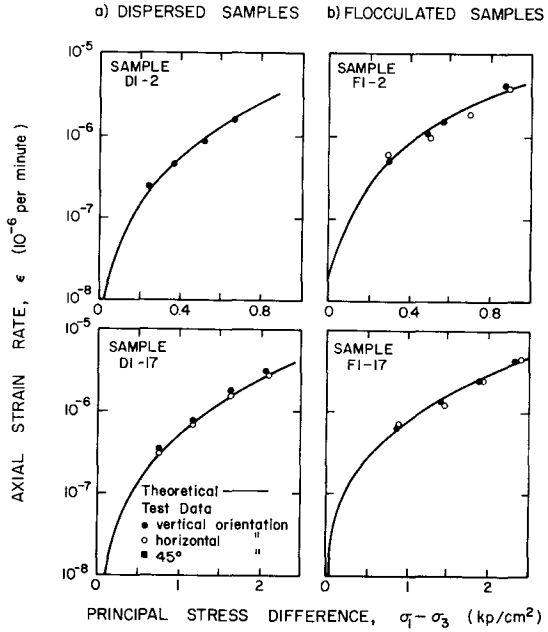

FIG. 13.—Fig. 11 Replotted in Semilog Scale (1 kp/cm² = 0.0981 N/mm²)

1 for the specimens tested. Essentially the same value of m was obtained for both vertically and horizontally trimmed specimens (as well as for the single 45° specimen tested) from the same consolidated sample. However, as shown in Fig. 9, m does vary with the void ratio of a sample and there is a distinct difference in the values of m for specimens trimmed from anisotropically consolidated (oriented) samples and for specimens trimmed from isotropically consolidated (random) samples. Specimens with a random fabric exhibit higher values of m than those with a preferred orientation of particles.

Stress-Dependence of Creep.—The straight-line relationship between the logarithm of strain rate and the logarithm of time was observed for all specimens tested, and plots similar to the one shown in Fig. 8 were used to evaluate

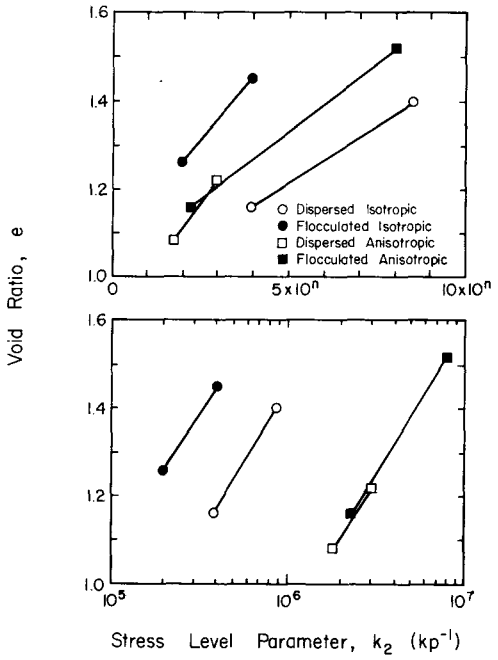

FIG. 14.—Influence of Void Ratio on Stress Level Parameter (1 kp = 9.81 N) (n = 5 for isotropic samples; n = 6 for anisotropic samples)

the strain rates at different stress levels for any given time to study the effect of stress on strain rate. Values of the parameter, k_2 (Eq. 15), for each sample are given in Table 1.

Comparisons of Experimental and Theoretical Results.—Creep curves were computed for a number of values for the material parameters, k_1 and k_2, and the values that provide the optimum fit of the test data were determined. The corresponding theoretical curves are compared with the test data in Figs. 10, 11, 12, and 13, and good agreement is found, except for one specimen (the horizontally trimmed specimen from sample FA-2) which showed excessive deformation during creep testing. Sample FA-2 was an extremely soft sample and the specimen was probably disturbed while setting up the test. Figs. 10

and 11 show the stress versus strain rate plots (both theoretical curves and experimental data) at 1,000 min after the application of each stress for all specimens tested. To demonstrate the stress dependence of strain rate at very low stress levels, a logarithmic strain rate versus stress plot is preferable. Figs. 12 and 13 show such plots, where strain rates are again selected at 1,000 min after application of each stress increment.

Although the strain rate decreases as the stress decreases, the rate of decrease becomes much more rapid for values of stress less than about one-half of the strength. Creep deformations at very small stress levels are very difficult to measure in the laboratory, but they probably do occur in nature, and the theoretical curves in Figs. 10 and 11 suggest the trend that may be expected at such stress levels. The variation of the parameter, k_2, which can be termed a stress level parameter, with void ratio for both anisotropically consolidated and isotropically consolidated samples from dispersed and flocculated slurries, is shown in Fig. 14.

To reduce the cost of computation, the curves in the foregoing figures were calculated by a simplified procedure, which assumes that the stress dependent parameter, k_2, is the same for all planes normal to the prevalent particle orientation. This can be true only when the same state of stress exists on all of these planes. However, based on a comparison with values determined by the correct procedure for specimens manifesting the greatest anisotropy, it was found that maximum differences in k_2 values are less than 20%. Thus, it seems acceptable to use the aforementioned simplified and less expensive procedure to calculate k_2, as was done herein.

Conclusions

Within the scope and limitations of the study presented herein, the following conclusions can be advanced.

1. The micromechanics model is capable of predicting the directional variations in the creep rate of anisotropic clays.
2. The model predicts the stress dependence of the creep rate without implying, in contrast with previous works (10,11), the simplifying assumption that the microscopic stresses that produce particle sliding are all equal.
3. The anisotropy of the clay fabric may be characterized by the probability density of the particle orientation distribution obtained from x-ray diffraction analyses; this reduces greatly the number of creep tests that must be performed to determine the anisotropy of creep behavior.
4. The material parameters in the mathematical model are dependent on the void ratio of the clay, the chemistry of the pore fluid, and the consolidation stress path.

Acknowledgments

This research was supported in large part by the National Science Foundation under Grant 18945-GCK, entitled "Effect of Soil Fabric on Engineering Properties." The x-ray diffraction tests were performed at the University of Illinois at Chicago Circle by K. S. Chawla with the help and cooperation of D. W. Baker.

Appendix I.—References

1. Baker, D. W., Wenk, A. R., and Christie, J. M., "X-ray Analysis of Preferred Orientation in Fine Grained Quartz Aggregates," *Journal of Geology*, Vol. 77, 1969, pp. 144-172.
2. Christensen, R. W., and Wu, T. H., "Analysis of Clay Deformation as a Rate Process," *Journal of the Soil Mechanics and Foundations Division*, ASCE, Vol. 90, No. SM6, Proc. Paper 4147, Nov., 1964, pp. 125-127.
3. Cottrell, A. H., *The Mechanical Properties of Matter*, John Wiley and Sons, Inc., New York, N.Y., 1964.
4. Diamond, S., "Pore Size Distribution in Clays," *Clays and Clay Minerals*, Vol. 18, 1970, pp. 7-23.
5. Edil, T. B., "Influence of Fabric and Soil Water Potential on Stress-Strain Response of Clay," thesis presented to Northwestern University, at Evanston, Ill. in 1973, in partial fulfillment of the requirements for the degree of Doctor of Philosophy.
6. Fung, Y. C., *Foundations of Solid Mechanics*, Prentice-Hall, Inc., Englewood Cliffs, N.J., 1965.
7. Glasstone, S., Laidler, K. J., and Eyring, H., *The Theory of Rate Processes*, McGraw-Hill Book Co., Inc., New York, N.Y., 1941.
8. Krizek, R. J., Edil, T. B., and Ozaydin, I. K., "Preparation and Identification of Clay Samples with Controlled Fabric," *Engineering Geology*, 1975 (in press).
9. Malmeister, A. K., "Fundamentals of the Theory of Local Strains" (in Russian), *Mekhanika Polymerov*, Vol. 5, No. 1, 1969, Riga, U.S.S.R., p. 22.
10. Mitchell, J. K., "Shearing Resistance of Soils as a Rate Process," *Jour. of the Soil Mechanics and Foundations Division*, ASCE, Vol. 90, No. SM1, Proc. Paper 3773, Jan., 1964, pp. 29-61.
11. Mitchell, J. K., Campanella, R. G., and Singh, A., "Soil Creep as a Rate Process," *Jour. of the Soil Mechanics and Foundations Division*, ASCE, Vol. 94, No. SM1, Proc. Paper 5751, Jan., 1968, pp. 231-253.
12. Sheeran, D. E., and Krizek, R. J., "Preparation of Homogeneous Soil Samples by Slurry Consolidation," *Jour. of Materials*, American Society for Testing and Materials, Vol. 6, 1971, pp. 356-373.
13. Singh, A., and Mitchell, J. K., "General Stress-Strain-Time Function for Soils," *Journal of the Soil Mechanics and Foundations Division*, ASCE, Vol. 94, No. SM1, Proc. Paper 5728, Jan., 1968, pp. 21-26.
14. Tan, T. K., "Structure Mechanics of Clays," *Academia Sinica*, Soil Mechanics Laboratory, Institute of Civil Engineering and Architecture, Harbin, China, 1957.
15. Tullis, T. E., "Experimental Development of Preferred Orientation of Mica During Recrystallization," thesis presented to the University of California, at Los Angeles, Calif., in 1971, in partial fulfillment of the requirements for the degree of Doctor of Philosophy.
16. Zienkiewicz, O. C., *The Finite Element Method in Engineering Science*, McGraw Hill Book Co., Inc., New York, N.Y., 1971.

Appendix II.—Notation

The following symbols are used in this paper:

$\mathbf{A}$ = incremental rate parameter in Eqs. 18 and 19:
$\mathbf{b}$ = matrix defined by Eq. 12;
$\mathbf{B}$ = matrix defined by Eq. 4;
$\mathbf{c}$ = matrix defined by Eq. 7;
$\mathbf{D}$ = matrix defined by Eq. 14;
k_c = parameter defined after Eq. 22;
k_0, k_1, k_2, m = creep parameters in Eqs. 15 and 17;
$N(\theta), N^*(\alpha)$ = particle orientation cumulative distribution and its planar projection (Eqs. 29 and 30);

$p(\Delta)$ = pore size density distribution (Eqs. 28 and 29);
$\mathbf{S}, S_i$ = slip forces in interparticle contacts (Eq. 15, Fig. 2);
$\mathbf{S}^0$ = nonviscous slip forces (Eqs. 18 and 19);
t = time;
$\mathbf{u}, \mathbf{u}_i, u_{x_i}, u_{y_i}$ = particle edge displacements (Eq. 1, Fig. 2);
$\mathbf{v}, v_i$ = slip velocities in interparticle contacts (Eq. 7);
x, y, z = cartesian axes, of which x is normal to prevalent particle orientation (Fig. 5);
x', y', z' = axes of the creep specimen (Fig. 5);
α_i, α = planar particle orientation angle (Fig. 2) and projected angle of normal to particle in space (Fig. 4);
$\beta, \beta_{ij}, \gamma$ = matrices in Eqs. 10, 11, 13;
$\tilde{\Delta}$ = area of triangular cell, Fig. 2;
$\underset{\sim}{\epsilon}, \epsilon_x, \epsilon_y, \gamma_{xy}$ = strain column matrix and its components (Eq. 2);
$\underset{\sim}{\dot{\epsilon}}^0$ = nonviscous strain rate (Eq. 20);
$\underset{\sim}{\eta}$ = incremental viscosity matrix (Eq. 20);
$\underset{\sim}{\sigma}$ = column matrix of macroscopic stresses (Eq. 20); and
$\underset{\sim}{\sigma}^0$ = nonviscous stress (Eq. 20).

Superscripts

$^-$ = quantities for tangential linearization of stress-strain relations;
$\cdot$ = time derivatives;
^{T} = transpose of a matrix; and
$'$ = components referred to axes x', y', z' (Fig. 5).

11138 MICROMECHANICS MODEL FOR CREEP OF CLAY

KEY WORDS: **Anisotropy;** Clay minerals; **Clays; Creep; Creep tests;** Elasticity; **Engineering mechanics;** Geotechnical engineering; **Mechanics;** Microstructure; **Particle spectra; Soil mechanics;** Stress strain characteristics;

ABSTRACT: Clays frequently possess a fabric with a preferred particle orientation and the creep properties of such clays are therefore anisotropic. A two-dimensional microstructural model to describe this creep response is developed. The model is based on a triangular cell of three particles sliding over each other at a rate predicted by rate-process theory. Equating the rate of energy dissipation within the cell to that of the macroscopic continuum leads to the determination of the tangential viscosity matrix and the matrix of the nonviscous stress components, both of which are stress dependent. The anisotropic creep viscosity parametres then are obtained by a statistical averaging procedure based on the probability density of the particle orientation distribution, as determined by x-ray diffraction. The resulting model is able to predict the directional differences in the creep rate and the stress dependence of creep in clays with anisotropic fabric. Undrained creep tests were conducted on specimens cut in various directions from both isotropically and anisotropically consolidated kaolinite samples.

REFERENCE: Bazant, Zdenek P., Ozaydin, I. Kutay, and Krizek, Raymond J., "Micromechanics Model for Creep of Anisotropic Clay," *Journal of the Engineering Mechanics Division,* ASCE, Vol. 101, No. EM1, **Proc. Paper 11138**, February, 1975, pp. 57-78